Transcrustal magmatic controls on the size of porphyry copper systems – State of knowledge and open questions

Cyril Chelle-Michou[1], Bertrand Rottier[2,3]

[1] Department of Earth Sciences, ETH Zürich, Clausiusstrasse 25, 8092 Zürich, Switzerland
[2] Département de Géologie et Génie Géologique, Université Laval, Québec, QC G1V 0A6, Canada [3] Centre de recherche sur la géologie et l'ingénierie des ressources minérales (E4m), Québec, Canada

cyril.chelle-michou@erdw.ethz.ch; bertrand.rottier@ggl.ulaval.ca

SUPPLEMENTARY TEXT AND FIGURES

Method for modelling

Table S1. List of symbols

Symbol	Description
C_A^{melt}	Mass concentration of element or compound *A* in the melt (in wt% for SiO_2, TiO_2, Al_2O_3, FeO, MnO, MgO, CaO, Na_2O, K_2O and H_2O; in ppm for Cl, S and Cu)
$C_A^{crystals}$	Mass concentration of element *A* in silicate and Fe-Ti oxide crystals (in ppm for Cl and Cu)
C_A^{fluid}	Mass concentration of element or compound *A* in the fluid (in wt% for NaCl, H_2S and SO_2; in ppm for Cl, S and Cu)
C_A^{MSS}	Mass concentration of element *A* in MSS (in ppm for Cu)
M_A	Molar weight of element or compound *A*
X_A^{melt}	Molar fraction of element or compound *A* in the melt
X_A^{fluid}	Molar fraction of element or compound *A* in the fluid
F	Melt fraction in the subsystem melt + crystals
m_{melt}	Mass fraction of melt in the magma
$m_{crystals}$	Mass fraction of silicate and Fe-Ti oxide crystals in the magma
m_{fluid}	Mass fraction of aqueous fluid in the magma
m_{MSS}	Mass fraction of monosulfide solid solution (MSS) in the magma
m_{anh}	Mass fraction of anhydrite in the magma
m_{H2O}	Mass fraction of degassed water in the magma
m_{NaCl}	Mass fraction of degassed NaCl in the magma (ignoring the presence of HCl, KCl and $FeCl_2$ in the fluid)
m_{SO2}	Mass fraction of degassed SO_2 in the magma
m_{H2S}	Mass fraction of degassed H_2S in the magma
$D_A^{\frac{fluid}{melt}}$	Mass partition coefficient of element *A* between fluid and melt
$D_A^{\frac{crystals}{melt}}$	Mass partition coefficient of element *A* between silicate and Fe-Ti oxide crystals and melt

$D_A^{\frac{MSS}{melt}}$	Mass partition coefficient of element *A* between MSS and melt
$D_A^{\frac{anhydrite}{melt}}$	Mass partition coefficient of element *A* between anhydrite and melt
D_A	Bulk partition coefficient of element *A* between the segregating phases (silicate and Fe-Ti oxide crystals, fluid, MSS, anhydrite) and melt
$r^{fluid}_{\frac{H2S}{H2S+SO2}}$	Mass ratio of H_2S to total S species in the fluid (assuming only H_2S and SO_2 are present)
$r^{fluid}_{\frac{SO2}{H2S+SO2}}$	Mass ratio of SO_2 to total S species in the fluid (assuming only H_2S and SO_2 are present)

We parametrized the melt composition and melt fraction (*F*) along the liquid line of descent obtained at 200 MPa by Marxer and Ulmer (2019) between 1000 and 700 °C using quintic functions (except for TiO_2 for which a quartic function was used). The polynomial regressions were anchored to normative minimum melt composition of Qz/Ab/Or = 35/40/25 at 680 °C and 200 MPa (Johannes and Holtz, 1996).

Sulfur concentration at sulfide saturation (SCSS in ppm) and at anhydrite saturation (SCAS in ppm) where computed according to Fortin et al. (2015) and Zajacz and Tsay (2019) for reduced ($[S^{2-}/S_{tot}]_{melt}$ = 1) and oxidized ($[S^{6+}/S_{tot}]_{melt}$ = 1) conditions, respectively. At intermediate oxygen fugacity, the speciation of sulfur in the melt and the corresponding SCSS or SCAS were computed following Jugo et al. (2010) and Botcharnikov et al. (2011). For numerical practicality (see Eqs. 23,24 below) we added binary parameters b_{SCSS} and b_{SCAS} which equal 1 if SCSS ≤ SCAS and SCAS < SCSS, respectively, and 0 otherwise.

The partition coefficient of sulfur between fluid and melt ($D_S^{fluid/melt}$) for typical arc magma compositions was parametrized using the experimental data of Zajacz et al. (2012, 2013) and Masotta et al. (2016). For oxygen fugacity equal or below the nickel-nickel oxide buffer (NNO), $D_S^{fluid/melt}$ shows to be a simple function of the molar proportion of FeO in the melt (X_{FeO}). The regression yields:

$$\ln D_S^{\frac{fluid}{melt}} = 5.29(\pm 0.03) - 2.75(\pm 0.15) \cdot X_{FeO} + + 0.46(\pm 0.15) \cdot (X_{FeO})^2 \quad (1)$$

with a residual standard error (RSE) of 0.15 (Fig. S1). In turn, under more oxidizing conditions (ΔNNO > 0), the dependence of $D_S^{fluid/melt}$ on melt composition writes as:

$$\ln D_S^{\frac{fluid}{melt}} = 3.90(\pm 0.08) - 9.4(\pm 2.5) \cdot \frac{NBO}{T} - 20(\pm 6) \cdot ASI - 36(\pm 10) \cdot ALK - 4.84(\pm 0.76) \cdot Al_{\#} - 36(\pm 12) \cdot Ca_{\#} \quad (2)$$

with a RSE of 0.47 (Fig. S1), where NBO/T refers to the nonbridging oxygens/tetrahedral cations in the silicate melt:

$$\frac{NBO}{T} = \frac{X_{Na}^{melt} + X_K^{melt} + 2 \cdot \left(X_{Ca}^{melt} + X_{Mg}^{melt} + X_{Fe}^{melt}\right) - X_{Al}^{melt}}{X_{Si}^{melt} + X_{Al}^{melt}} \quad (3)$$

ASI and ALK refer to the aluminum saturation index and the alkalinity of the melt, respectively:

$$ASI = \frac{X_{Al2O3}^{melt}}{X_{CaO}^{melt} + X_{Na2O}^{melt} + X_{K2O}^{melt}} \tag{4}$$

$$ALK = \frac{X_{Na2O}^{melt} + X_{K2O}^{melt}}{X_{Al2O3}^{melt}} \tag{5}$$

and *Al#* and *Ca#* are compositional parameters inspired from Masotta et al. (2016):

$$Al_{\#} = \frac{X_{Al2O3}^{melt}}{X_{SiO2}^{melt} + X_{TiO2}^{melt} + X_{Al2O3}^{melt}} \tag{6}$$

$$Ca_{\#} = \frac{X_{CaO}^{melt}}{X_{CaO}^{melt} + X_{Na2O}^{melt} + X_{K2O}^{melt}} \tag{7}$$

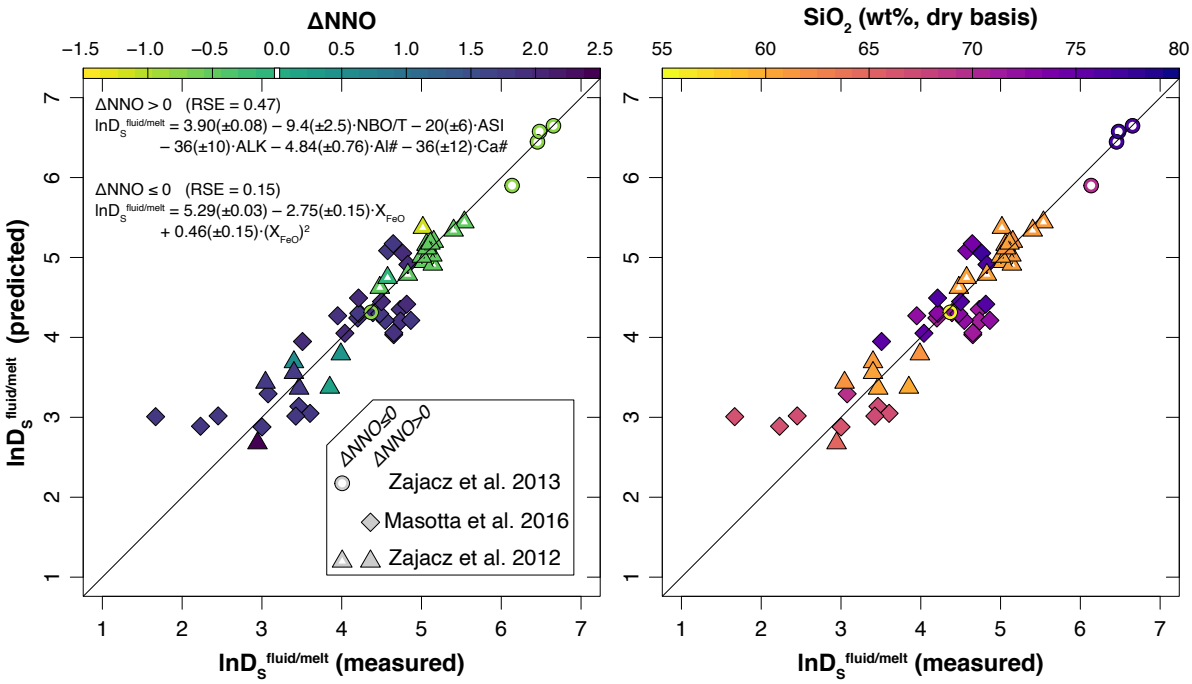

Figure S1. Plot of measured vs predicted $D_S^{fluid/melt}$ using Eqs. 1 and 2 colored according to the ΔNNO of the experiment (left) and the SiO_2 concentration of the melt. RSE: residual standard error of the regression.

Sulfur speciation in the fluid was computed as a function of oxygen fugacity, temperature and pressure using the equilibrium constant of the reaction $2 \cdot SO_2(g) + 2 \cdot H_2O(g) = 2 \cdot H_2S(g) + 3 \cdot O_2$ determined experimentally by Binder and Keppler (2011).

The partition coefficient of chlorine between fluid and melt ($D_{Cl}^{fluid/melt}$) for typical arc magma compositions was parametrized using the experimental data of Simon et al. (2004), Zajacz et al. (2012), and Botcharnikov et al. (2004, 2007, 2015) and yield:

$$\ln D_{Cl}^{\frac{fluid}{melt}} = 4.26(\pm 0.77) + 0.50(\pm 0.03) \cdot \ln \mu Cl_{fluid} + 0.59(\pm 0.13) \cdot \ln P - 6.53(\pm 0.49) \cdot \frac{NBO}{T} - 4.37(\pm 0.62) \cdot ASI \tag{8}$$

with a RSE of 0.38 (Fig. S2), where μCl_{fluid} is the Cl molality of the fluid (mol/kg H_2O) and P is the pressure in MPa.

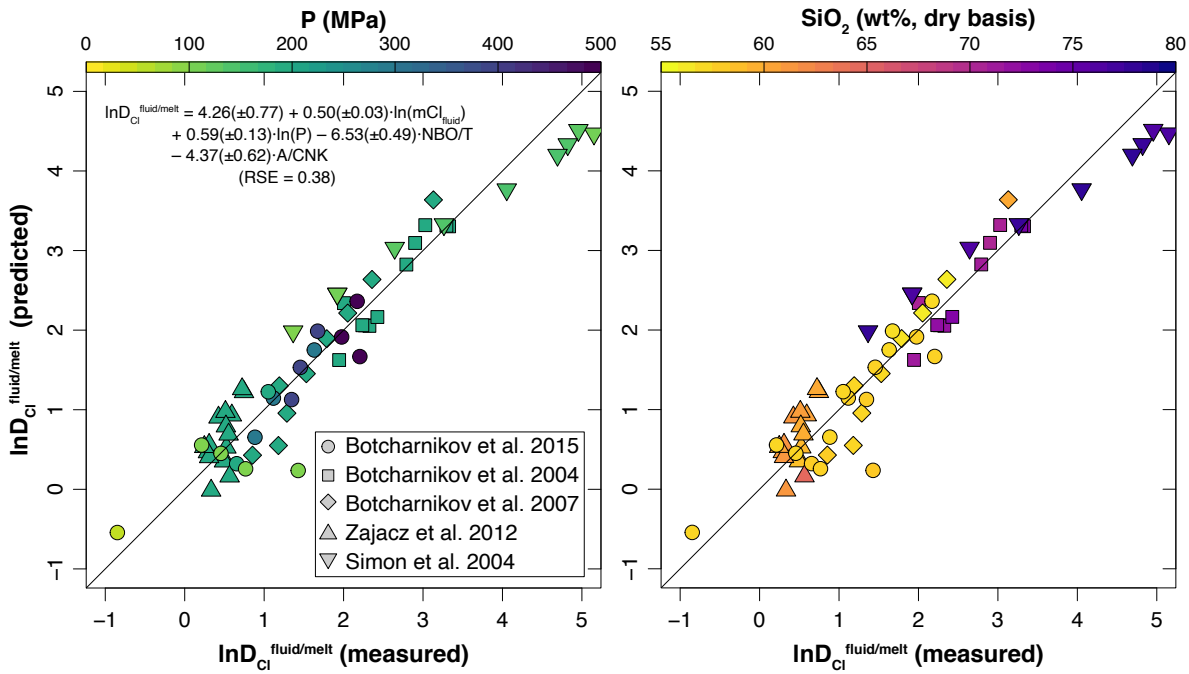

Figure S2. Plot of measured vs predicted $D_{Cl}^{fluid/melt}$ using Eq. 8 colored according to the pressure of the experiment (left) and the SiO_2 concentration of the melt. RSE: residual standard error of the regression.

Each model run starts at the point of water saturation. At the beginning of each run, let us consider 1 g of magma containing melt ± crystals. Previous models of degassing have considered S and Cl to behave are trace elements (e.g., Chelle-Michou et al., 2017). This resulted in the approximation that the contribution of their respective species (i.e., SO_2, H_2S and NaCl) to the mass of the fluid phase remain negligible (i.e., $m_{fluid} = m_{water}$). Here, we employ a more rigorous approach whereby the partitioning of S and Cl in the fluid (in the form of SO_2, H_2S and NaCl) impact on the mass of the fluid and of the melt. S and Cl partitioning between melt and the segregating phases (silicates, fluid, anhydrite and MSS) was computed in two stages as follows. At start, we assume that no anhydrite or MSS saturate. At each step the mass conservation writes as:

$$m_{melt_i} = 1 - m_{crytals_i} - m_{fluid_i} \tag{9}$$

$$m_{fluid_i} = m_{water_i} + m_{SO2_i} + m_{H2S_i} + m_{NaCl_i} \tag{10}$$

Where the input F_i is defined as:

$$F_i = \frac{m_{melt_i}}{m_{melt_i} + m_{crytals_i}} \tag{11}$$

$$m_{water_i} = \frac{C_{H2O}^{melt}}{10^2} \cdot \left(m_{melt_0} - m_{melt_i}\right) \tag{12}$$

$$\frac{C_{SO2}^{fluid}{}_i}{10^6} = \frac{m_{SO2_i}}{m_{fluid_i}} = \frac{C_S^{fluid}{}_i}{10^6} \cdot \frac{M_S + 2M_O}{M_S} \cdot r^{fluid}_{\frac{SO2}{H2S+SO2}_i} \tag{13}$$

$$\frac{C_{H2S}^{fluid}{}_i}{10^6} = \frac{m_{H2S_i}}{m_{fluid_i}} = \frac{C_S^{fluid}{}_i}{10^6} \cdot \frac{2M_H + M_S}{M_S} \cdot r_{\frac{H2S}{H2S+SO2}_i}^{fluid} \tag{14}$$

$$\frac{C_{NaCl}^{fluid}{}_i}{10^6} = \frac{m_{NaCl_i}}{m_{fluid_i}} = \frac{C_{Cl}^{fluid}{}_i}{10^6} \cdot \frac{M_{Na} + M_{Cl}}{M_{Cl}} \tag{15}$$

The bulk partition coefficient for S and Cl between melt and the segregating phases (crystals and fluid) writes as

$$D_{S_i} = D_S^{\frac{fluid}{melt}}{}_i \cdot \frac{m_{fluid_i}}{1 - m_{melt_i}} \tag{16}$$

$$D_{Cl_i} = D_{Cl}^{\frac{fluid}{melt}}{}_i \cdot \frac{m_{fluid_i}}{1 - m_{melt_i}} + D_{Cl}^{\frac{crystals}{melt}}{}_i \cdot \frac{m_{crystals_i}}{1 - m_{melt_i}} \tag{17}$$

with $D_{Cl}^{\frac{crystals}{melt}} = 0.1$ to account for the partitioning of Cl in amphibole and biotite. Considering an equilibrium fractionation model, the concentration of Cl and S in melt at any step is given by:

$$C_S^{melt}{}_i = \frac{C_S^{melt}{}_0}{D_{S_i} + m_{melt_i} \cdot (1 - D_{S_i})} \tag{18}$$

$$C_{Cl}^{melt}{}_i = \frac{C_{Cl}^{melt}{}_0}{D_{Cl_i} + m_{melt_i} \cdot (1 - D_{Cl_i})} \tag{19}$$

The corresponding concentrations in the equilibrated fluid phase are

$$C_S^{fluid}{}_i = C_S^{melt}{}_i \cdot D_S^{\frac{fluid}{melt}}{}_i \tag{20}$$

$$C_{Cl}^{fluid}{}_i = C_{Cl}^{melt}{}_i \cdot D_{Cl}^{\frac{fluid}{melt}}{}_i \tag{21}$$

The system of non-linear equations Eqs. 8–21 with 14 unknowns was solved at each degassing step using a Newton method. At the second stage, if $C_S^{melt}{}_i$ exceeds SCAS or SCSS, $C_S^{melt}{}_i$ is fixed to the minimum of the two values and $C_S^{fluid}{}_i$ is recalculated according to Eq. 20. The excess sulfur is partitioned into anhydrite or MSS. In such case, the mass conservation writes as:

$$m_{melt_i} = 1 - m_{crytals_i} - m_{fluid_i} - m_{anh_i} - m_{MSS_i} \tag{22}$$

With

$$m_{anh_i} = b_{SCAS_i} \cdot \frac{C_S^{melt}{}_0 \cdot 1 - C_S^{melt}{}_i \cdot m_{melt_i} - C_S^{fluid}{}_i \cdot m_{fluid_i}}{10^6} \cdot \frac{M_{Ca} + M_S + 4M_O}{M_S} \tag{23}$$

$$m_{MSS_i} = b_{SCSS_i} \cdot \frac{C_S^{melt}{}_0 \cdot 1 - C_S^{melt}{}_i \cdot m_{melt_i} - C_S^{fluid}{}_i \cdot m_{fluid_i}}{10^6} \cdot \frac{M_{Fe} + M_S}{M_S} \tag{24}$$

The new system of non-linear equations defined by Eqs. 8,10–15,17,19,21,22–24 with 13 unknowns was solved using the same Newton method as before.

In contrast to S and Cl, Cu was treated as a trace element able to partition between melt, silicates, MSS, and fluid. The partition coefficient of Cu between silicates + Fe-Ti oxide and melt was fixed at 0.2 (following Liu et al., 2015). The partitioning of Cu between MSS and melt, and fluid and melt were according to Li and Audétat (2015) and Tattitch and Blundy (2017), respectively. The bulk partition coefficient for Cu writes as:

$$D_{Cu_i} = D_{Cu}^{\frac{fluid}{melt}}{}_i \cdot \frac{m_{fluid_i}}{1 - m_{melt_i}} + D_{Cu}^{\frac{crystals}{melt}}{}_i \cdot \frac{m_{crystals_i}}{1 - m_{melt_i}} + D_{Cu}^{\frac{MSS}{melt}}{}_i \cdot \frac{m_{MSS_i}}{1 - m_{melt_i}}$$

and the evolution of the Cu concentration in the melt is:

$$C_{Cu}^{melt}{}_i = \frac{C_{Cu}^{melt}{}_0}{D_{Cu_i} + m_{melt_i} \cdot (1 - D_{Cu_i})}$$

from which we can calculate the concentrations of Cu in the different phases.

References

Binder, B., and Keppler, H., 2011, The oxidation state of sulfur in magmatic fluids: Earth and Planetary Science Letters, v. 301, p. 190–198.

Botcharnikov, R. E., Behrens, H., Holtz, F., Koepke, J., and Sato, H., 2004, Sulfur and chlorine solubility in Mt. Unzen rhyodacitic melt at 850 °C and 200 MPa: Chemical Geology, v. 213, p. 207–225.

Botcharnikov, R. E., Holtz, F., and Behrens, H., 2007, The effect of CO2 on the solubility of H2O-Cl fluids in andesitic melt: European Journal of Mineralogy, v. 19, p. 671–680.

Botcharnikov, R. E., Linnen, R. L., Wilke, M., Holtz, F., Jugo, P. J., and Berndt, J., 2011, High gold concentrations in sulphide-bearing magma under oxidizing conditions: Nature Geoscience, v. 4, p. 112–115.

Botcharnikov, R. E., Holtz, F., and Behrens, H., 2015, Solubility and fluid–melt partitioning of H2O and Cl in andesitic magmas as a function of pressure between 50 and 500MPa: Chemical Geology, v. 418, p. 117–131.

Chelle-Michou, C., Rottier, B., Caricchi, L., and Simpson, G., 2017, Tempo of magma degassing and the genesis of porphyry copper deposits.: Scientific reports, v. 7, p. 40566.

Fortin, M.-A., Riddle, J., Desjardins-Langlais, Y., and Baker, D. R., 2015, The effect of water on the sulfur concentration at sulfide saturation (SCSS) in natural melts: Geochimica et Cosmochimica Acta, v. 160, p. 100–116.

Johannes, W., and Holtz, F., 1996, Petrogenesis and Experimental Petrology of Granitic Rocks: Minerals and Rocks, Berlin, Heidelberg, Springer, 335 p.

Jugo, P. J., Wilke, M., and Botcharnikov, R. E., 2010, Sulfur K-edge XANES analysis of natural and synthetic basaltic glasses: Implications for S speciation and S content as function of oxygen fugacity: Geochimica et Cosmochimica Acta, v. 74, p. 5926–5938.

Li, Y., and Audétat, A., 2015, Effects of temperature, silicate melt composition, and oxygen fugacity on the partitioning of V, Mn, Co, Ni, Cu, Zn, As, Mo, Ag, Sn, Sb, W, Au, Pb, and Bi between sulfide phases and silicate melt: Geochimica et Cosmochimica Acta, v. 162, p. 25–45.

Liu, X., Xiong, X., Audétat, A., and Li, Y., 2015, Partitioning of Cu between mafic minerals, Fe–Ti oxides and intermediate to felsic melts: Geochimica et Cosmochimica Acta, v. 151, p. 86–102.

Marxer, F., and Ulmer, P., 2019, Crystallisation and zircon saturation of calc-alkaline tonalite from the Adamello Batholith at upper crustal conditions: an experimental study: Contributions to Mineralogy and Petrology, v. 174, p. 84.

Masotta, M., Keppler, H., and Chaudhari, A., 2016, Fluid-melt partitioning of sulfur in differentiated arc magmas and the sulfur yield of explosive volcanic eruptions: Geochimica et Cosmochimica Acta, v. 176, p. 26–43.

Simon, A. C., Pettke, T., Candela, P. A., Piccoli, P. M., and Heinrich, C. A., 2004, Magnetite solubility and iron transport in magmatic-hydrothermal environments: Geochimica et Cosmochimica Acta, v. 68, p. 4905–4914.

Tattitch, B. C., and Blundy, J. D., 2017, Cu-Mo partitioning between felsic melts and saline-aqueous fluids as a function of XNaCleq, $fO2$, and $fS2$: American Mineralogist, v. 102, p. 1987–2006.

Zajacz, Z., and Tsay, A., 2019, An accurate model to predict sulfur concentration at anhydrite saturation in silicate melts: Geochimica et Cosmochimica Acta, v. 261, p. 288–304.

Zajacz, Z., Candela, P. A., Piccoli, P. M., and Sanchez-Valle, C., 2012, The partitioning of sulfur and chlorine between andesite melts and magmatic volatiles and the exchange coefficients of major cations: Geochimica et Cosmochimica Acta, v. 89, p. 81–101.

Zajacz, Z., Candela, P. A., Piccoli, P. M., Sanchez-Valle, C., and Wälle, M., 2013, Solubility and partitioning behavior of Au, Cu, Ag and reduced S in magmas: Geochimica et Cosmochimica Acta, v. 112, p. 288–304.